Received: 18 February 2019 | Revised: 18 November 2019 | Accepted: 18 November 2019

DOI: 10.1002/zamm.201900050

ORIGINAL PAPER

An implementation and numerical experiments of the FEM-BEM coupling for the elastodynamic wave equation in 3D

Sarah Eberle

Institute for Mathematics, Goethe-University Frankfurt, Frankfurt am Main, Germany

Correspondence
Sarah Eberle, Institute for Mathematics, Goethe-University Frankfurt, Frankfurt am Main, Germany.
Email: eberle@math.uni-frankfurt.de

In this paper we deal with an implementation as well as numerical experiments for the coupling of interior and exterior problems of the elastodynamic wave equation with transparent boundary conditions in 3D as described in a previous paper by this author. In more detail, the FEM-BEM-coupling as well as the time discretization by using leapfrog and convolution quadrature is considered. Our aim is to provide an insight into the necessary steps of the implementation. Based on this, we present numerical experiments for a non-convex domain and analyze the errors.

KEYWORDS
convolution quadrature, elastodynamic wave equation, FEM-BEM-coupling, leapfrog, numerical experiments

1 | INTRODUCTION AND OUTLINE

In recent times, the FEM-BEM coupling for partial differential equations gained more and more importance. It first appeared in a paper by Zienkiewicz et al.[20] and was later build upon by Li et al.[15] Its application is manifold, such as, e.g., crack problems in fracture mechanics (Aour et al.[3]), ground-structure interaction (Jean[11]), and for the dynamics of flexible bodies (Kerdjouj and Amirouche[12]). Major topics of research include the acoustic (cf. Banjai et al.,[4] Sayas,[18] Clouteau et al.,[6] and Ziegelwanger et al.[19]) and elastic wave equation. Specifically for the elastic wave equation, relevant publications for this paper are Carstensen et al.,[5] dealing with a 2d elastic transmission problem, Domínguez et al.,[7] describing the general 2d elastic Calderón operator and presenting a 2d scattering problem, as well as Kielhorn and Schanz[14] analysing 3d static and dynamic elastic problems with prescribed boundary conditions.

In continuation of the article by Eberle,[8] this work is intended to add to the ongoing research by presenting the implementation and numerical realization of the FEM-BEM coupling of the elastodynamic wave equation in 3D for transparent boundary conditions. As such this paper is the first to complete the union of theory and numerics for this problem. We start our consideration by summarizing the theoretical results of the stable numerical coupling of interior and exterior problems for the elastodynamic wave equation given in Eberle,[8] which provides the basis for the implementation. We present the results of the discretization itself and also take a look at the results concerning the stability and convergence of the numerical methods. After that, we go over to the implementation, where we want to remark that there already exist implementations for the elastodynamic wave equation, which deal with parts of our problem, e.g., the FEM part by either Alberty et al.[1] in Matlab, or C++-libraries from FEniCs (cf. Alnaes et al.[2]), as well as the C++-libraries HyENA by Schanz (see, e.g. Kielhorn and Schanz[14]) for the BEM part. To our knowledge there is no implementation for the elastodynamic wave equation with tranparent boundary conditions which couples the corresponding time discretization for finite and boundary elements. But we want to mention the work by

Rammerstorfer and Schanz[16] and Rüberg and Schanz[17] concerning the FEM-BEM coupling for other elasticity problems as well as for fluid problems by Estorff and Antes.[9] Thus, this paper plays an essential role in the numerical/theoretical treatment of the transient elasticity problem with transparent boundary conditions. Concerning the implementation, we first take a look at the generation of the meshes with respect to the finite and boundary elements. After that, we go over to the construction of the matrix, where we split our consideration into the parts which belong to the boundary, interior and coupling terms, and also highlight their special treatment, e.g. for the boundary the regularization of the strong and hypersingular kernel which appear in the BEM formulation. In the last section, we present numerical experiments for a non-convex domain and the corresponding error plots. We close our paper with a summary and conclusion.

2 | THE ELASTODYNAMIC WAVE EQUATION

In order to introduce the problem of interest, we recapitulate the background from Eberle.[8] Thus, we take a look at the three-dimensional elastodynamic wave equation given by

$$\rho\partial_t^2 u = \mu\Delta u + (\lambda+\mu)\nabla(\nabla\cdot u) + \rho\partial_t f \quad \text{in } \mathbb{R}^3\times[0,T], \tag{2.1}$$

where u ist the displacement vector, ρ the density, λ and μ the Lamé parameter and $\rho\partial_t f$ the force. In addition, we prescribe the initial conditions

$$\begin{aligned} u(\cdot,0) &= u_0 \quad \text{in } \mathbb{R}^3,\\ \partial_t u(\cdot,0) &= v_0 \quad \text{in } \mathbb{R}^3, \end{aligned}$$

where f, u_0 and v_0 are compactly supported. This problem statement implies the following radiation condition due to the finite speed of wave propagation: $u(\cdot,t)$ is compactly supported for all t.

Our aim is to construct a stable numerical method, which couples the interior and exterior problem for a non-convex domain Ω. Therefore, we split the problem in the following way.

Problem in interior space:

$$\begin{aligned} \rho\partial_t^2 u^- &= \mu\Delta u^- + (\lambda+\mu)\nabla(\nabla\cdot u^-) + \rho\partial_t f \qquad \text{in } \Omega\times[0,T],\\ u^-(\cdot,0) &= u_0 \quad \text{in } \Omega,\\ \partial_t u^-(\cdot,0) &= v_0 \quad \text{in } \Omega. \end{aligned}$$

Problem in exterior space:

$$\begin{aligned} \rho\partial_t^2 u^+ &= \mu\Delta u^+ + (\lambda+\mu)\nabla(\nabla\cdot u^+), \quad \text{in } \Omega^+\times[0,T],\\ u^+(\cdot,0) &= 0 \quad \text{in } \Omega^+,\\ \partial_t u^+(\cdot,0) &= 0 \quad \text{in } \Omega^+, \end{aligned}$$

with $\Omega^+ = \mathbb{R}^3\setminus\overline{\Omega}$.

Transmission conditions:

$$\begin{aligned} \gamma^- u^- &= \gamma^+ u^+,\\ \mathcal{T}^- u^- &= \mathcal{T}^+ u^+. \end{aligned}$$

Here, γ^- and γ^+ represent the interior and exterior traces on the boundary $\partial\Omega=\Gamma$ and $\mathcal{T}^-$ and $\mathcal{T}^+$ denote the stress operator for the interior and exterior case, which is given by

$$\mathcal{T}u = \sigma(u)n = (2\mu\varepsilon(u) + \lambda(\nabla\cdot u)I)n,$$

where $\varepsilon(u) = \frac{1}{2}(\nabla u + (\nabla u)^T)$.

2.1 | The Calderón operator

Next, we go over to the construction of the Calderón operator and proceed in the same way as in Eberle.[8] First, we take a look at the Laplace transformed wave equation

$$\rho s^2 u = \mu \Delta u + (\lambda + \mu)\nabla(\nabla \cdot u) + \rho s f + \rho s u_0 + \rho v_0$$

with the parameter $s \in \mathbb{C}$.

We introduce the fundamental solution given by (see, e.g., Kielhorn[13])

$$\hat{G}(x-y,s) = \frac{1}{\mu}\left[\Delta_x \chi(|x-y|,s) I - \frac{\lambda+\mu}{\lambda+2\mu}\nabla_x \nabla_x \chi(|x-y|,s)\right] - \frac{1}{\mu}k_1(s)^2 \chi(|x-y|,s) I, \tag{2.2}$$

with

$$\chi(|x-y|,s) := \frac{1}{4\pi}\frac{1}{k_1(s)^2 - k_2(s)^2}\frac{\exp(-k_1(s)|x-y|) - \exp(-k_2(s)|x-y|)}{|x-y|}, \tag{2.3}$$

$$k_1(s) = s\sqrt{\frac{\rho}{\lambda+2\mu}} \quad \text{and} \quad k_2(s) = s\sqrt{\frac{\rho}{\mu}}. \tag{2.4}$$

In order to construct the Calderón operator, we define the boundary densities

$$\psi = -[\gamma u] \quad \text{on } \Gamma,$$

$$\phi = \frac{1}{s}[\mathcal{T} u] \quad \text{on } \Gamma,$$

where $[\gamma u] = \gamma^- u - \gamma^+ u$ and $[\mathcal{T} u] = \mathcal{T}^- u - \mathcal{T}^+ u$ are the jumps in the boundary traces.

After that, we apply the operators γ and $\mathcal{T}$ to the ansatz

$$u = sS(s)\phi + D(s)\psi,$$

where $S(s)$ is the single layer potential and $D(s)$ the double layer potential given by

$$S(s)\phi(x) = \int_\Gamma \hat{G}(x-y,s)\phi(y)\, d\Gamma_y,$$

$$D(s)\phi(x) = \int_\Gamma \mathcal{T}_y \hat{G}(x-y,s)\phi(y)\, d\Gamma_y \quad \text{for } x \in \mathbb{R}^3 \setminus \Gamma.$$

This leads to

$$\begin{pmatrix} [\gamma \cdot] \\ \frac{1}{s}[\mathcal{T} \cdot] \end{pmatrix} \begin{pmatrix} sS(s)\phi & D(s)\psi \end{pmatrix} = \begin{pmatrix} 0 & -\psi \\ s\phi & 0 \end{pmatrix}$$

due to the limit and jump relations of the operators $[\gamma \cdot]$ and $\frac{1}{s}[\mathcal{T} \cdot]$ (see Eberle[8]).

Observing the boundary integral operators in the Laplace domain given by

$$J(s)\phi(x) = \int_\Gamma \hat{G}(x-y,s)\phi(y) d\Gamma_y,$$

$$K^T(s)\phi(x) = \int_\Gamma \left(\mathcal{T}_y \hat{G}(x-y,s)\right)\phi(y) d\Gamma_y,$$

$$K(s)\phi(x) = \mathcal{T}_x \int_\Gamma \hat{G}(x-y,s)\phi(y) d\Gamma_y,$$

$$W(s)\phi(x) = -\mathcal{T}_x \int_\Gamma \left(\mathcal{T}_y \hat{G}(x-y,s)\right)\phi(y) d\Gamma_y \quad \text{for } x \in \Gamma,$$

the averages $\{\{\cdot\}\}$ are defined by

$$\begin{aligned} J(s)\phi &= \{\{\gamma S(s)\phi\}\} = \gamma^{\pm} S(s)\phi, \\ K(s)\phi &= \{\{\mathcal{T} S(s)\phi\}\}, \\ K^T(s)\psi &= \{\{\gamma D(s)\psi\}\}, \\ W(s)\psi &= -\{\{\mathcal{T} D(s)\psi\}\} = -\mathcal{T}^{\pm} D(s)\psi, \end{aligned}$$

which results in

$$\begin{pmatrix} \{\{\gamma\cdot\}\} \\ -\frac{1}{s}\{\{\mathcal{T}\cdot\}\} \end{pmatrix} \begin{pmatrix} sS(s)\phi & D(s)\psi \end{pmatrix} = \begin{pmatrix} sJ(s)\phi & K^T(s)\psi \\ -K(s)\phi & \frac{1}{s}W(s)\psi \end{pmatrix},$$

so that we define the Calderón operator $B(s)$ as

$$B(s) = \begin{pmatrix} sJ(s) & K^T(s) \\ -K(s) & \frac{1}{s}W(s) \end{pmatrix}. \tag{2.5}$$

Next, we present the coercivity results for the Calderón operator, which play an important role for the stability analysis.

We start with the Laplace domain followed by the time domain and the reader should note that the proofs can be found in Eberle.[8]

Lemma 1 (Eberle [8], Lemma 1). *There exists $\tilde{\beta} > 0$ such that the Calderón operator $B(s)$ satisfies*

$$\operatorname{Re}\left\langle \begin{pmatrix} \phi \\ \psi \end{pmatrix}, B(s) \begin{pmatrix} \phi \\ \psi \end{pmatrix} \right\rangle_{\Gamma} \geq \operatorname{Re} s\, \tilde{\beta} \frac{1}{|s|^2} \min\left(1, |s|^2\right) \left(\|\phi\|^2_{H^{-\frac{1}{2}}(\Gamma)^3} + \|\psi\|^2_{H^{\frac{1}{2}}(\Gamma)^3} \right)$$

for $\operatorname{Re} s > 0$ and for all $\phi \in H^{-\frac{1}{2}}(\Gamma)^3$ and $\psi \in H^{\frac{1}{2}}(\Gamma)^3$.

This lemma is the basis for the stability analysis of the numerical methods and applied in the framework of the energy considerations.

Given the discrete convolution

$$B(\partial_t) \begin{pmatrix} \phi \\ \psi \end{pmatrix} = \frac{1}{2} \begin{pmatrix} \gamma^- u^- \\ -\partial_t^{-1} \mathcal{T}^- u^- \end{pmatrix}$$

with ∂_t^{-1} as the antiderivative presented in Eberle,[8] we directly get the next lemma by the inverse Laplace transformation applied to Lemma 1.

Lemma 2 (Eberle [8], Lemma 5). *With the constant $\tilde{\beta}$ from Lemma 1, we have*

$$\int_0^T e^{-\frac{2t}{T}} \left\langle \begin{pmatrix} \phi(\cdot,t) \\ \psi(\cdot,t) \end{pmatrix}, B(\partial_t) \begin{pmatrix} \phi \\ \psi \end{pmatrix}(\cdot,t) \right\rangle_{\Gamma} dt \geq \tilde{\beta} c_T \int_0^T e^{-\frac{2t}{T}} \left(\|\partial_t^{-1}\phi(\cdot,t)\|^2_{H^{-\frac{1}{2}}(\Gamma)^3} + \|\partial_t^{-1}\psi(\cdot,t)\|^2_{H^{\frac{1}{2}}(\Gamma)^3} \right),$$

for any $T > 0$ and for all $\phi \in C^4([0,T], H^{-\frac{1}{2}}(\Gamma)^3)$ and all $\psi \in C^3([0,T], H^{\frac{1}{2}}(\Gamma)^3)$ with $\phi(\cdot,0) = \partial_t\phi(\cdot,0) = \cdots = \partial_t^3\phi(\cdot,0) = 0$, $\psi(\cdot,0) = \partial_t\phi(\cdot,0) = \partial_t^2\phi(\cdot,0) = 0$. Here, $c_T = \min(T^{-1}, T^{-3})$.

In order to close this part, we finally take a look at the behavior of the energy over time.

Lemma 3 (Eberle [8], Lemma 6). *Let $E : [0,\infty) \to [0,\infty)$, $S : \mathbb{R} \to \mathbb{R}$, $\phi \in C^4([0,T], H^{-\frac{1}{2}}(\Gamma)^3)$, $\psi \in C^3([0,T], H^{\frac{1}{2}}(\Gamma)^3)$ with $\phi(\cdot,0) = \partial_t\phi(\cdot,0) = \partial_t^2\phi(\cdot,0) = \partial_t^3\phi(\cdot,0) = 0$, $\psi(\cdot,0) = \partial_t\psi(\cdot,0) = \partial_t^2\psi(\cdot,0) = 0$. If*

$$\dot{E} + \left\langle \begin{pmatrix} \phi \\ \psi \end{pmatrix}, B(\partial_t) \begin{pmatrix} \phi \\ \psi \end{pmatrix} \right\rangle_{\Gamma} = S \qquad \text{in } [0,T],$$

then

$$E(T)+\tilde{\beta}c_T\int_0^T\left(\|\partial_t^{-1}\phi(\cdot,t)\|^2_{H^{-\frac{1}{2}}(\Gamma)^3}+\|\partial_t^{-1}\psi(\cdot,t)\|^2_{H^{\frac{1}{2}}(\Gamma)^3}\right)dt\le e^2E(0)+\int_0^T e^{2(1-\frac{t}{T})}S(t)\,dt,$$

where $c_T=\min(T^{-1},T^{-3})$.

Later on, $E(t)$ will be the field energy introduced in the next section.

3 | DISCRETIZATION

Now, we go over to the space and time discretization, where a detailed description again can be found in Eberle.[8] We want to remark that due to the coupling, we only have to solve the problem in $\overline{\Omega}$. Thus, we will consider FEM and leapfrog in the interior and BEM with convolution quadrature on the boundary.

3.1 | Background of the space discretization

In order to formulate the weak formulation, which we need for the finite element method in the interior, we transform the elastic wave equation (2.1) into the first order system

$$\begin{aligned}\rho\partial_t u&=\mu\nabla\cdot V+\lambda\nabla\omega+\rho f,\\ \partial_t V&=2\varepsilon(u),\\ \partial_t\omega&=\nabla\cdot u,\\ B(\partial_t)\begin{pmatrix}\phi\\ \psi\end{pmatrix}&=\frac{1}{2}\begin{pmatrix}\gamma u\\ -\gamma(\mu V+\lambda\omega I)n\end{pmatrix}.\end{aligned}$$

For the sake of readability, we write $(\cdot,\cdot)$ instead of the inner products $(\cdot,\cdot)_{L^2(\mathbb{R}^3\setminus\Gamma)}$, $(\cdot,\cdot)_{L^2(\mathbb{R}^3\setminus\Gamma)^3}$ and $(\cdot,\cdot)_{L^2(\mathbb{R}^3\setminus\Gamma)^{3\times3}}$ from now on, since the type of the scalar product will be clear from context. Partial integration leads to the weak formulation

$$\begin{aligned}\rho(\partial_t u,z)=&-\frac{1}{2}\mu(V,\nabla z)+\frac{1}{2}\mu(\nabla\cdot V,z)+\frac{1}{2}\mu\langle\gamma Vn,\gamma z\rangle_\Gamma\\ &-\frac{1}{2}\lambda(\omega,\nabla\cdot z)+\frac{1}{2}\lambda(\nabla\omega,z)+\frac{1}{2}\lambda\langle\gamma(\omega I)n,\gamma z\rangle_\Gamma+\rho(f,z),\\ (\partial_t V,Y)=&(\varepsilon(u),Y)-(u,\varepsilon^*(Y))+\frac{1}{2}\langle\gamma u,\gamma(Y+Y^T)n\rangle_\Gamma,\\ (\partial_t\omega,x)=&-\frac{1}{2}(u,\nabla x)+\frac{1}{2}(\nabla\cdot u,x)+\frac{1}{2}\langle\gamma u,\gamma(xI)n\rangle_\Gamma,\\ \left\langle\begin{pmatrix}\xi\\ \eta\end{pmatrix},B(\partial_t)\begin{pmatrix}\phi\\ \psi\end{pmatrix}\right\rangle_\Gamma=&\frac{1}{2}\langle\xi,\gamma u\rangle_\Gamma-\frac{1}{2}\langle\eta,\gamma(\mu V)n\rangle_\Gamma-\frac{1}{2}\langle\eta,\gamma(\lambda\omega I)n\rangle_\Gamma,\end{aligned}$$

where $\varepsilon^*(Y):\mathbb{R}^{3\times3}\to\mathbb{R}^3$, $\varepsilon^*(Y):=\frac{1}{2}\nabla\cdot(Y+Y^T)$, $z:\mathbb{R}^3\to\mathbb{R}^3$, $Y:\mathbb{R}^3\to\mathbb{R}^{3\times3}$, $x:\mathbb{R}^3\to\mathbb{R}$, and $\xi,\eta:\mathbb{R}^3\to\mathbb{R}^3$.

Testing with $z=u$, $Y=\frac{\mu}{2}V$, $x=\lambda\omega$, $\xi=\phi$, $\eta=\psi$ and adding the four equations, we finally arrive at

$$\frac{d}{dt}\left(\frac{1}{2}\rho\|u\|^2_{L_2(\Omega)^3}+\frac{1}{4}\mu\|V\|^2_{L_2(\Omega)^{3\times3}}+\frac{1}{2}\lambda\|\omega\|^2_{L_2(\Omega)}\right)+\left\langle\begin{pmatrix}\phi\\ \psi\end{pmatrix},B(\partial_t)\begin{pmatrix}\phi\\ \psi\end{pmatrix}\right\rangle_\Gamma=\rho(f,u)_{L_2(\Omega)^3}.$$

For $\rho,\ \mu,\ \lambda>0$, which is valid for most common materials, and the positivity result of the Calderón operator $B(\partial_t)$ from Lemma 2, this provides that the field energy

$$E=\frac{1}{2}\rho\|u\|^2_{L_2(\Omega)^3}+\frac{1}{4}\mu\|V\|^2_{L_2(\Omega)^{3\times3}}+\frac{1}{2}\lambda\|\omega\|^2_{L_2(\Omega)}$$

satisfies

$$E(t) + \tilde{\beta} c_T \int_0^T \left(\|\partial_t^{-1} \phi(\cdot,t)\|^2_{H^{-\frac{1}{2}}(\Gamma)^3} + \|\partial_t^{-1} \psi(\cdot,t)\|^2_{H^{\frac{1}{2}}(\Gamma)^3} \right) dt \leq e^2 E(0) \tag{3.1}$$

for $t > 0$ and $f = 0$. Equation (3.1) shows that the energy decreases over time and is smaller than the initial energy $E(0)$. It should be noted that the field energy in the sense of this paper is not an energy in the physical sense. However, its time derivative provides the kinetic and potential energy of the wave.

This builds the basis for the convergence examination, where we adopt this result to the discrete energy consideration.

We couple the spacial discretization of the interior with the one performed on the boundary, which leads to the FEM-BEM coupling. With $\partial_t u = \dot{u}$, $\partial_t V = \dot{V}$, $\partial_t \omega = \dot{\omega}$, the system is valid for the nodal values of the variables.

$$\rho \mathbf{M_0} \dot{\mathbf{u}} = -\mu \mathbf{D}^{\mathrm{T}} \mathbf{V} + \lambda \overline{\mathbf{D}} \omega - \mathbf{C_0} \boldsymbol{\phi} + \rho \mathbf{M_0} \mathbf{f}, \tag{3.2}$$

$$\mathbf{M_1} \dot{\mathbf{V}} = \mathbf{D}\mathbf{u} - \mathbf{C_1} \boldsymbol{\psi}, \tag{3.3}$$

$$\mathbf{M_2} \dot{\boldsymbol{\omega}} = -\overline{\mathbf{D}}^{\mathrm{T}} \mathbf{u} - \overline{\mathbf{C}}_1 \boldsymbol{\psi}, \tag{3.4}$$

$$\mathbf{B}(\partial_t) \begin{pmatrix} \boldsymbol{\phi} \\ \boldsymbol{\psi} \end{pmatrix} = \begin{pmatrix} \mathbf{C}_0^{\mathrm{T}} \mathbf{u} \\ \mu \mathbf{C}_1^{\mathrm{T}} \mathbf{V} + \lambda \overline{\mathbf{C}}_1^{\mathrm{T}} \omega \end{pmatrix}. \tag{3.5}$$

Now, let $\mathcal{W}_h$, $\mathcal{U}_h$, $\mathcal{V}_h$, Ψ_h, and Φ_h be finite dimensional subspaces of the Sobolev spaces: $\mathcal{W}_h \subset H^1(\Omega)$, $\mathcal{U}_h = \mathcal{W}_h^3 \subset H^1(\Omega)^3$, $\mathcal{V}_h = \mathcal{W}_h^{3\times 3} \subset H^1(\Omega)^{3\times 3}$, $\Psi_h \subset H^{\frac{1}{2}}(\Gamma)^3$, and $\Phi_h \subset H^{-\frac{1}{2}}(\Gamma)^3$. Here, $\mathcal{W}_h$ is a finite element space of piecewise linear function, Ψ_h the boundary element space of piecewise linear functions, and Φ_h the boundary element space of piecewise constant functions. In addition, $b_j^{\mathcal{U}}$, $b_j^{\mathcal{V}}$, $b_j^{\mathcal{W}}$ and b_j^{Ψ} are piecewise linear and b_j^{Φ} piecewise constant basis functions of the respective spaces for the tetrahedra and triangles.

Thus, we have

$$\mathbf{D}|_{ij} = \frac{1}{2}(b_i^{\mathcal{V}}, \nabla b_j^{\mathcal{U}}) - \frac{1}{2}(\nabla \cdot b_i^{\mathcal{V}}, b_j^{\mathcal{U}}), \qquad \overline{\mathbf{D}}|_{ij} = \frac{1}{2}(b_i^{\mathcal{U}}, \nabla b_j^{\mathcal{W}}) - \frac{1}{2}(\nabla \cdot b_i^{\mathcal{U}}, b_j^{\mathcal{W}}),$$

$$\mathbf{M_0}|_{ij} = (b_i^{\mathcal{U}}, b_j^{\mathcal{U}}), \qquad \mathbf{M_1}|_{ij} = \frac{1}{2}(b_i^{\mathcal{V}}, b_j^{\mathcal{V}}), \qquad \mathbf{M_2}|_{ij} = (b_i^{\mathcal{W}}, b_j^{\mathcal{W}}),$$

$$\mathbf{C_0}|_{ij} = -\frac{1}{2}\left\langle b_j^{\Phi}, \gamma b_i^{\mathcal{U}} \right\rangle_{\Gamma}, \qquad \mathbf{C_1}|_{ij} = \frac{1}{2}\left\langle b_j^{\Psi}, \gamma b_i^{\mathcal{V}} n \right\rangle_{\Gamma}, \qquad \overline{\mathbf{C}}_1|_{ij} = \frac{1}{2}\left\langle b_j^{\Psi}, \gamma b_i^{\mathcal{W}} n \right\rangle_{\Gamma},$$

$$\mathbf{J}(s)|_{ij} = \left\langle b_i^{\Phi}, J(s) b_j^{\Phi} \right\rangle_{\Gamma}, \qquad \mathbf{K}(s)|_{ij} = \left\langle b_i^{\Phi}, K(s) b_j^{\Psi} \right\rangle_{\Gamma}, \quad \mathbf{W}(s)|_{ij} = \left\langle b_i^{\Psi}, W(s) b_j^{\Psi} \right\rangle_{\Gamma}.$$

In order to close the consideration of the full discretization, we take a look at the time discretization. We apply a leapfrog scheme in the interior of the domain and a convolution quadrature method on the boundary (see Eberle[8]) so that we have

$$\mathbf{M_1} \mathbf{V}^{n+\frac{1}{2}} = \mathbf{M_1} \mathbf{V}^n + \frac{1}{2} \triangle t \mathbf{D} \mathbf{u}^n - \frac{1}{2} \triangle t \mathbf{C_1} \boldsymbol{\psi}^n, \tag{3.6}$$

$$\mathbf{M_2} \boldsymbol{\omega}^{n+\frac{1}{2}} = \mathbf{M_2} \boldsymbol{\omega}^n - \frac{1}{2} \triangle t \overline{\mathbf{D}}^{\mathrm{T}} \mathbf{u}^n - \frac{1}{2} \triangle t \overline{\mathbf{C}}_1 \boldsymbol{\psi}^n, \tag{3.7}$$

$$\rho \mathbf{M_0} \mathbf{u}^{n+1} = \rho \mathbf{M_0} \mathbf{u}^n - \mu \triangle t \mathbf{D}^{\mathrm{T}} \mathbf{V}^{n+\frac{1}{2}} + \lambda \triangle t \overline{\mathbf{D}} \boldsymbol{\omega}^{n+\frac{1}{2}} + \rho \triangle t \mathbf{M_0} \mathbf{f}^{n+\frac{1}{2}} - \triangle t \mathbf{C_0} \boldsymbol{\phi}^{n+\frac{1}{2}}, \tag{3.8}$$

$$\mathbf{M_1} \mathbf{V}^{n+1} = \mathbf{M_1} \mathbf{V}^{n+\frac{1}{2}} + \frac{1}{2} \triangle t \mathbf{D} \mathbf{u}^{n+1} - \frac{1}{2} \triangle t \mathbf{C_1} \boldsymbol{\psi}^{n+1}, \tag{3.9}$$

$$\mathbf{M_2} \boldsymbol{\omega}^{n+1} = \mathbf{M_2} \boldsymbol{\omega}^{n+\frac{1}{2}} - \frac{1}{2} \triangle t \overline{\mathbf{D}}^{\mathrm{T}} \mathbf{u}^{n+1} - \frac{1}{2} \triangle t \overline{\mathbf{C}}_1 \boldsymbol{\psi}^{n+1}, \tag{3.10}$$

$$\left[\mathbf{B}(\partial_t^{\triangle t}) \begin{pmatrix} \boldsymbol{\phi} \\ \overline{\boldsymbol{\psi}} \end{pmatrix} \right]^{n+\frac{1}{2}} = \begin{pmatrix} \mathbf{C}_0^{\mathrm{T}} \overline{\mathbf{u}}^{\mathbf{n}+\frac{1}{2}} \\ \mu \mathbf{C}_1^{\mathrm{T}} \left(\mathbf{V}^{n+\frac{1}{2}} - \alpha \triangle t^2 \mathbf{M_1^{-1}} \mathbf{C_1} \dot{\boldsymbol{\psi}}^{n+\frac{1}{2}} \right) + \lambda \overline{\mathbf{C}}_1^{\mathrm{T}} \left(\boldsymbol{\omega}^{n+\frac{1}{2}} - \alpha \triangle t^2 \mathbf{M_2^{-1}} \overline{\mathbf{C}}_1 \dot{\boldsymbol{\psi}}^{n+\frac{1}{2}} \right) \end{pmatrix}, \tag{3.11}$$

where $\overline{\mathbf{u}}^{n+\frac{1}{2}} = \frac{1}{2}(\mathbf{u}^{n+1} + \mathbf{u}^n)$, $\overline{\boldsymbol{\psi}}^{n+\frac{1}{2}} = \frac{1}{2}(\boldsymbol{\psi}^{n+1} + \boldsymbol{\psi}^n)$ and $\alpha > 0$ is a stabilization parameter, so that for $\overline{\mathbf{u}}^{n+\frac{1}{2}}$ and $\overline{\boldsymbol{\psi}}^{n+\frac{1}{2}}$, we have

$$\overline{\mathbf{u}}^{n+\frac{1}{2}} = \frac{1}{2}\left(2\mathbf{u}^n - \mu\frac{\triangle t}{\rho}\mathbf{M}_\mathbf{0}^{-1}\mathbf{D}^\mathrm{T}\mathbf{V}^{n+\frac{1}{2}} + \lambda\frac{\triangle t}{\rho}\mathbf{M}_\mathbf{0}^{-1}\overline{\mathbf{D}}\omega^{n+\frac{1}{2}} - \frac{\triangle t}{\rho}\mathbf{M}_\mathbf{0}^{-1}\mathbf{C}_\mathbf{0}\boldsymbol{\phi}^{n+\frac{1}{2}} + \triangle t\mathbf{f}^{n+\frac{1}{2}}\right), \tag{3.12}$$

$$\triangle t\dot{\boldsymbol{\psi}}^{n+\frac{1}{2}} = 2\overline{\boldsymbol{\psi}}^{n+\frac{1}{2}} - 2\boldsymbol{\psi}^n. \tag{3.13}$$

In addition, we have to take the CFL-condition into account. Hence, we convert the system into

$$\tilde{\mathbf{M}}_\mathbf{0}\dot{\mathbf{u}} = -\tilde{\mathbf{D}}^\mathrm{T}\mathbf{Z} - \mathbf{C}_\mathbf{0}\boldsymbol{\phi} + \tilde{\mathbf{M}}_\mathbf{0}\mathbf{f},$$

$$\tilde{\mathbf{M}}\dot{\mathbf{Z}} = \tilde{\mathbf{D}}\mathbf{u} - \tilde{\mathbf{C}}_\mathbf{1}\boldsymbol{\psi},$$

$$\mathbf{B}(\partial_t)\begin{pmatrix}\boldsymbol{\phi}\\ \boldsymbol{\psi}\end{pmatrix} = \begin{pmatrix}\mathbf{C}_\mathbf{0}^\mathrm{T}\mathbf{u}\\ \tilde{\mathbf{C}}_\mathbf{1}^\mathrm{T}\mathbf{Z}\end{pmatrix}$$

with

$$\tilde{\mathbf{M}}_\mathbf{0} = \rho\mathbf{M}_\mathbf{0}, \quad \tilde{\mathbf{M}} = \begin{pmatrix}\mu\mathbf{M}_\mathbf{1} & \mathbf{0}\\ \mathbf{0} & \lambda\mathbf{M}_\mathbf{2}\end{pmatrix}, \quad \mathbf{Z} = \begin{pmatrix}\mathbf{V}\\ \boldsymbol{\omega}\end{pmatrix}, \quad \tilde{\mathbf{D}} = \begin{pmatrix}\mu\mathbf{D}\\ -\lambda\overline{\mathbf{D}}^\mathrm{T}\end{pmatrix}, \quad \tilde{\mathbf{C}}_\mathbf{1} = \begin{pmatrix}\mu\mathbf{C}_\mathbf{1}\\ \lambda\overline{\mathbf{C}}_\mathbf{1}\end{pmatrix}.$$

This allows us to borrow the CFL condition from Banjai et al.[4] and their calculation of the CFL condition from the acoustic wave equation, so that by observing the transformation, we directly obtain from the acoustic case

$$\triangle t\|\tilde{\mathbf{M}}^{-\frac{1}{2}}\tilde{\mathbf{D}}\tilde{\mathbf{M}}_\mathbf{0}^{-\frac{1}{2}}\|_2 \leq 1.$$

In addition, the lower bound on the stabilization parameter is given by

$$\alpha \geq 1.$$

Finally, we summarize the error bound for the fully discretized problem as well as its convergence, which is stated in the next theorem (see Eberle[8]). This theorem is very important because it shows the optimal-order error bounds of the full discretization with $\mathcal{O}(h)$ in space and $\mathcal{O}(\triangle t^2)$ in time.

Theorem 4 (Eberle [8], Theorem 3). *Assume that the initial values and the inhomogeneity of the wave equation have their support in Ω. Let the initial values for the semi-discretization be chosen as $u_h(0) = P_h u(0)$, $V_h(0) = P_h V(0)$, $\omega_h(0) = P_h\omega(0)$, where P_h denotes the L_2-orthogonal projection onto the respective finite element spaces. If the solution of the wave equation is sufficiently smooth, then the error of the FEM and BEM with leapfrog and convolution quadrature full discretization under the CFL condition and the stability parameter α is bounded at $t = n\triangle t$ by*

$$\begin{aligned}&\rho\|u_h^n - u(t)\|_{L_2(\Omega)^3} + \frac{1}{2}\mu\|V_h^n - V(t)\|_{L_2(\Omega)^{3\times 3}} + \lambda\|\omega_h^n - \omega(t)\|_{L_2(\Omega)}\\ &+\left(\triangle t\sum_{j=0}^{n-1}\|\phi_h^{j+\frac{1}{2}} - \phi(t_{j+\frac{1}{2}})\|^2_{H^{-\frac{1}{2}}(\Gamma)^3} + \|\overline{\psi}_h^{j+\frac{1}{2}} - \psi(t_{j+\frac{1}{2}})\|^2_{H^{\frac{1}{2}}(\Gamma)^3}\right)^{\frac{1}{2}}\\ &\leq C(t)(h + \triangle t^2),\end{aligned}$$

where the constant $C(t)$ grows at most polynomially with t.

Remark 1. For Theorem 4, we assume a sufficiently smooth boundary (i.e., a Lipschitz boundary), which we do not have in reality when we apply our implementation. However it turns out, that our numerical scheme computes a stable solution for our example if the time step size and the grid width is sufficiently small.

4 | IMPLEMENTATION

We start with a general overview of the different steps which have to be performed for the implementation. Thus, we provide a brief introduction of tetrahedral coordinates, followed by the construction of the matrices for the FEM-BEM coupling. After that, we take a closer look at the convolution quadrature.

For the implementation of the FEM-BEM approach, we use linear basis functions and tetrahedral elements. Hence, we apply the approach of the coordinate transformation given by Felippa[10] and transform the Cartesian coordinates into tetrahedral coordinates via

$$\begin{pmatrix} 1 \\ x \\ y \\ z \end{pmatrix} = \begin{pmatrix} 1 & 1 & 1 & 1 \\ x_1 & x_2 & x_3 & x_4 \\ y_1 & y_2 & y_3 & y_4 \\ z_1 & z_2 & z_3 & z_4 \end{pmatrix} \begin{pmatrix} \zeta_1 \\ \zeta_2 \\ \zeta_3 \\ \zeta_4 \end{pmatrix}. \tag{4.1}$$

Here, $(x_i, y_i, z_i)^T$, $i = 1, \dots, 4$, are the four nodal coordinates of the tetrahedron and $\zeta_i \in [0, 1]$, $i = 1, \dots, 4$, are the tetrahedral coordinates.

In order to calculate the required tetrahedral coordinates, we have to invert the system (4.1) so that

$$\begin{pmatrix} \zeta_1 \\ \zeta_2 \\ \zeta_3 \\ \zeta_4 \end{pmatrix} = \frac{1}{6V} \begin{pmatrix} 6V_{01} & y_{42}z_{32} - y_{32}z_{42} & x_{32}z_{42} - x_{42}z_{32} & x_{42}y_{32} - x_{32}y_{42} \\ 6V_{02} & y_{31}z_{43} - y_{34}z_{13} & x_{43}z_{31} - x_{13}z_{34} & x_{31}y_{43} - x_{34}y_{13} \\ 6V_{03} & y_{24}z_{14} - y_{14}z_{24} & x_{14}z_{24} - x_{24}z_{14} & x_{24}y_{14} - x_{14}y_{24} \\ 6V_{04} & y_{13}z_{21} - y_{12}z_{31} & x_{21}z_{13} - x_{31}z_{12} & x_{13}y_{21} - x_{12}y_{31} \end{pmatrix} \begin{pmatrix} 1 \\ x \\ y \\ z \end{pmatrix} \tag{4.2}$$

$$= \frac{1}{6V} \begin{pmatrix} 6V_{01} & a_1 & b_1 & c_1 \\ 6V_{02} & a_2 & b_2 & c_2 \\ 6V_{03} & a_3 & b_3 & c_3 \\ 6V_{04} & a_4 & b_4 & c_4 \end{pmatrix} \begin{pmatrix} 1 \\ x \\ y \\ z \end{pmatrix}, \tag{4.3}$$

where

$$\begin{aligned} 6V_{01} &= x_2(y_3z_4 - y_4z_3) + x_3(y_4z_2 - y_2z_4) + x_4(y_2z_3 - y_3z_2), \\ 6V_{02} &= x_1(y_4z_3 - y_3z_4) + x_3(y_1z_4 - y_4z_1) + x_4(y_3z_1 - y_1z_3), \\ 6V_{03} &= x_1(y_2z_4 - y_4z_2) + x_2(y_4z_1 - y_1z_4) + x_4(y_1z_2 - y_2z_1), \\ 6V_{04} &= x_1(y_3z_2 - y_2z_3) + x_2(y_1z_3 - y_3z_1) + x_3(y_2z_1 - y_1z_2), \end{aligned}$$

and

$$V = V_{01} + V_{02} + V_{03} + V_{04}. \tag{4.4}$$

Based on this, we continue with the spacial discretization and take a closer look at the system of the FEM-BEM coupling (3.2)-(3.5). We start with the boundary matrices, i.e., $\mathbf{J}$, $\mathbf{K}$ and $\mathbf{W}$, for the BEM part. For a given face of a terahedron Γ^e, these entries are calculated with the corresponding basis functions b^ϕ (piecewise constant) and b^ψ (piecewise linear) via

$$\mathbf{J}(s)|_{ij} = \left\langle b_i^\phi, J(s) b_j^\phi \right\rangle_\Gamma, \tag{4.5}$$

$$\mathbf{K}(s)|_{ij} = \left\langle b_i^\phi, K(s) b_j^\psi \right\rangle_\Gamma, \tag{4.6}$$

$$\mathbf{W}(s)|_{ij} = \left\langle b_i^\psi, W(s) b_j^\psi \right\rangle_\Gamma. \tag{4.7}$$

Here, we use

$$b_i^{\phi} = e_i, \qquad i = 1,2,3,$$
$$b_i^{\psi} = \zeta_{i-4\lfloor\frac{i-1}{4}\rfloor} e_{\lceil\frac{i}{4}\rceil}, \qquad i = 1,\dots,12,$$

where e_i is the i-th Euclidean unit vector.

In addition, the calculation of these boundary matrices involves the consideration of singular integrals. Thus, before we apply a suitable quadrature rule to calculate the boundary intergals, the singularities in $\mathbf{K}$ and $\mathbf{W}$ have to be regularized.

For the fundamental solution the reader is referred to Equation (2.2)–(2.4). We utilize the regularization for the strong and the hypersingular kernel from Kielhorn.[13] For $\Gamma = \partial\Omega$, we have for the operator K

$$\begin{aligned}(Ku)(x) =& 2\mu \int_\Gamma \hat{G}(x-y,s)\cdot(\mathcal{M}(\partial_y, n(y))u)\, d\Gamma_y - \int_\Gamma \Delta\chi\, \mathcal{M}(\partial_y, n(y))u)\, d\Gamma_y + \int_\Gamma \frac{\partial \Delta\chi}{\partial n(y)} u\, d\Gamma_y \\ &- \int_\Gamma \frac{d\chi}{dr}\left[(k_2^2 - 2k_1^2)\nabla_y r \otimes n(y) + k_1^2 n(y)\otimes\nabla_y r + k_1^2 \frac{\partial r}{\partial n(y)} I\right)\cdot u\, d\Gamma_y,\end{aligned} \tag{4.8}$$

where $\mathcal{M}(\partial_y, n(y))$ denotes the Günther derivatives given by

$$\mathcal{M}(\partial_n, n(y)) = \nabla_y \otimes n(y) - n(y)\otimes\nabla_y,$$

with $\otimes$ as the Kronecker product. As observed by Kielhorn and Schanz,[14] it should be noted that the last term of (4.8) is regular since

$$\frac{d\chi}{dr} = \frac{1}{8\pi}\frac{k_1^2 + k_1k_2 + k_2^2}{12(k_1+k_2)\pi} + \mathcal{O}(r^2).$$

Following Kielhorn,[13] the regularization of the hypersingular kernel W is obtained by taking a look at

$$(Wu)(\tilde{x}) = -\left(\mathcal{T}(\partial_{\tilde{x}}, n(x))(Ku)(\tilde{x}) - \frac{k_1^2}{\mu}\mathcal{T}(\partial_{\tilde{x}}, n(x)) \int_\Gamma \left[\mathcal{T}(\partial_y, n(y))\chi I\right]^T \cdot u\, d\Gamma_y\right), \tag{4.9}$$

where $\tilde{x}\in\Omega$, $x\in\Gamma$.

Given the surface curl

$$\frac{\partial}{\partial S(\partial_y, n(y))} = n(y)\times\nabla_y,$$

where $\frac{\partial}{\partial S_k(\partial_y, n(y))}$ denotes its k-th component, we consider the limit process $\tilde{x}\in\Omega$, $\tilde{x}\to x\in\Gamma$ in (4.9), so that by observing Stokes theorem, we get the weak singular kernel

$$\begin{aligned}\langle Wu, v\rangle_\Gamma =& 2\mu \int_\Gamma\int_\Gamma \Delta_y\chi \sum_{k,i=1}^{3} \frac{\partial u_i(y)}{\partial S_k(\partial_y, n(y))}\frac{\partial v_i(y)}{\partial S_k(\partial_y, n(y))} d\Gamma_y d\Gamma_x \\ &- \mu\int_\Gamma\int_\Gamma \Delta_y\chi \frac{\partial}{\partial S(\partial_y, n(y))}\cdot u(y)\frac{\partial}{\partial S(\partial_x, n(y))}\cdot v(y) d\Gamma_y d\Gamma_x \\ &- \mu\int_\Gamma\int_\Gamma (\mathcal{M}_x\cdot v(x))\cdot\left(4\mu\hat{G} - 2\Delta_y\chi I\right)\cdot(\mathcal{M}_y\cdot u(y)) d\Gamma_y d\Gamma_x \\ &+ \mu\int_\Gamma\int_\Gamma v(x)\cdot\left[(k_2^2 - 2k_1^2)(\Delta_y\chi - k_2^2\chi)n(x)\otimes n(y)\right]\cdot u(y) d\Gamma_y d\Gamma_x \\ &+ \mu\int_\Gamma\int_\Gamma v(x)\cdot\left[k_2^2(\Delta_y\chi - k_1^2\chi)n(y)\otimes n(x)\right]\cdot u(y) d\Gamma_y d\Gamma_x\end{aligned}$$

$$+\mu\int_\Gamma\int_\Gamma v(x)\cdot\left[(2(k_2^2-k_1^2)\nabla_y\nabla_y\chi+\Delta_y^2\chi I)n(y)\cdot n(x)\right]\cdot u(y)d\Gamma_y d\Gamma_x$$
$$+\mu\int_\Gamma\int_\Gamma v(x)\cdot\left[2k_2^2\mathcal{M}_x\cdot(\mathcal{M}_y\chi)+k_1^2\mathcal{M}_y\cdot(\mathcal{M}_x\chi)\right]\cdot u(y)d\Gamma_y d\Gamma_x$$
$$+\mu\int_\Gamma\int_\Gamma k_1^2\frac{\partial^2\chi}{\partial n(y)\partial n(x)}v(x)\cdot u(y)d\Gamma_y d\Gamma_x.$$

Using the regularized kernels, we are able to approximate the integrals via Gaussian quadrature.

Remark 2. We want to remark that there are also other regularization approaches since a regularization is not unique.

Next, we take a look at the entries for the interior, i.e., $\mathbf{M_0}$, $\mathbf{M_1}$, $\mathbf{M_2}$, $\mathbf{D}$, and $\overline{\mathbf{D}}$ for each terahedron Ω^e.
For the FEM part of the problem, we use the piecewise linear ansatz functions

$$\begin{aligned} b_i^{\mathcal{U}} &= \zeta_{i-4\lfloor\frac{i-1}{4}\rfloor}e_{\lceil\frac{i}{4}\rceil}, && i=1,\dots,12,\\ b_i^{\mathcal{V}} &= \zeta_{i-4\lfloor\frac{i-1}{4}\rfloor}e_{\lceil\frac{i}{4}\rceil-3\lfloor\frac{i-1}{12}\rfloor}e^T_{\lceil\frac{i}{12}\rceil}, && i=1,\dots,36,\\ b_i^{\mathcal{W}} &= \zeta_i, && i=1,\dots,4, \end{aligned}$$

in order to calculate

$$\mathbf{M_0}|_{ij}=(b_i^{\mathcal{U}},b_j^{\mathcal{U}}), \tag{4.10}$$

$$\mathbf{M_1}|_{ij}=\frac{1}{2}(b_i^{\mathcal{V}},b_j^{\mathcal{V}}), \tag{4.11}$$

$$\mathbf{M_2}|_{ij}=(b_i^{\mathcal{W}},b_j^{\mathcal{W}}). \tag{4.12}$$

Exemplary for $\mathbf{M_2}$ we have

$$(b_i^{\mathcal{W}},b_j^{\mathcal{W}})=\int_{\Omega^e}\zeta_i\zeta_j\,d\Omega^e=\begin{cases}\frac{1}{10}V, & \text{if} \quad i=j\\ \frac{1}{20}V, & \text{if} \quad i\neq j\end{cases},$$

where Ω^e is the tetrahedron in question and V given in (4.4).

For computing the matrices $\mathbf{D}$ and $\overline{\mathbf{D}}$ given by

$$\mathbf{D}|_{ij}=\frac{1}{2}(b_i^{\mathcal{V}},\nabla b_j^{\mathcal{U}})-\frac{1}{2}(\nabla\cdot b_i^{\mathcal{V}},b_j^{\mathcal{U}}), \tag{4.13}$$

$$\overline{\mathbf{D}}|_{ij}=\frac{1}{2}(b_i^{\mathcal{U}},\nabla b_j^{\mathcal{W}})-\frac{1}{2}(\nabla\cdot b_i^{\mathcal{U}},b_j^{\mathcal{W}}), \tag{4.14}$$

we need the representation of partial derivatives given by

$$6V\frac{\partial\zeta_i}{\partial x}=a_i,\quad 6V\frac{\partial\zeta_i}{\partial y}=b_i,\quad 6V\frac{\partial\zeta_i}{\partial z}=c_i,$$

with a_i, b_i and c_i from Equation (4.3) in addition to the basis functions. Since the gradient of $b_i^{\mathcal{U}}$, $b_i^{\mathcal{V}}$, $b_i^{\mathcal{W}}$ is constant, it should be noted that

$$\int_{\Omega^e}\zeta_i\,d\Omega^e=\frac{1}{4}V.$$

The coupling matrices $\mathbf{C_1}$ and $\overline{\mathbf{C}}_\mathbf{1}$ are given by

$$\mathbf{C_1}|_{ij} = \frac{1}{2}\left\langle b_j^{\Psi}, \gamma b_i^{\mathcal{V}} n\right\rangle_{\Gamma^e}, \tag{4.15}$$

$$\overline{\mathbf{C}}_\mathbf{1}|_{ij} = \frac{1}{2}\left\langle b_j^{\Psi}, \gamma b_i^{\mathcal{W}} n\right\rangle_{\Gamma^e}, \tag{4.16}$$

$$\mathbf{C_0}|_{ij} = -\frac{1}{2}\left\langle b_j^{\Phi}, \gamma b_i^{\mathcal{V}}\right\rangle_{\Gamma^e} \tag{4.17}$$

and can be calculated explicitly by use of tetrahedral coordinates. For the entries involving b_i^{Ψ} we have

$$\int_{\Gamma^e} \zeta_i \zeta_j \, d\Gamma^e = \begin{cases} \frac{1}{12} S, & \text{if} \quad i = j \\ \frac{1}{24} S, & \text{if} \quad i \neq j \end{cases},$$

where S is the surface area of the face Γ^e of the tetrahedron. For the entries concerning b_i^{ϕ}, we need the integral

$$\int_{\Gamma^e} \zeta_i \, d\Gamma^e = \frac{1}{6} S,$$

in order to calculate the matrix entries, since b_i^{ϕ} is piecewise constant. Then for each element, we calculate the entries of the local matrix according to (4.5)-(4.7) as well as (4.10)-(4.17) and sort those at the correct positions of the global matrices used in the time and space discretization later on.

Next, we come to the time discretization.

4.1 | Performance of the time discretization

For the time discretization, we split our considerations into the interior and the boundary, where we provide a detailed description for the convolution quadrature on the boundary, since the application of the leapfrog scheme is straight forward.

We recapitulate the leapfrog scheme given in (3.6)-(3.10), where

$$\mathbf{f}^{n+\frac{1}{2}} = \frac{1}{2}\left(\mathbf{f}^{n+1} + \mathbf{f}^{n}\right)$$

and the discrete values of $\boldsymbol{\psi}$ and $\boldsymbol{\phi}$ are obtained via convolution quadrature on the boundary.

For the convolution quadrature, we use the backward differentiation formula of order two (BDF2). The corresponding weights can be approximated by the trapezoidal rule. In more detail, we take a look at the system (3.11) and the discretization (3.12) and (3.13).

We have to consider the initial system at time $t = 0$ involving $\mathbf{B_0} = \mathbf{B}\left(\frac{\delta(0)}{\Delta t}\right)$. The theoretical background can be found in Eberle[8] and Kielhorn[13] and is based on a vector-valued version of the Herglotz Theorem. Thus, for the convolution quadrature, we have

$$\mathbf{B_0}\begin{pmatrix} \boldsymbol{\phi}_\mathbf{m} \\ \overline{\boldsymbol{\psi}}_\mathbf{m} \end{pmatrix} = \begin{pmatrix} \mathbf{b}_\mathbf{m}^{\phi} \\ \mathbf{b}_\mathbf{m}^{\psi} \end{pmatrix},$$

where

$$\begin{pmatrix} \mathbf{b}_\mathbf{m}^{\phi} \\ \mathbf{b}_\mathbf{m}^{\psi} \end{pmatrix} = \begin{pmatrix} \overline{\mathbf{b}}_\mathbf{m}^{\phi} \\ \overline{\mathbf{b}}_\mathbf{m}^{\psi} \end{pmatrix} - \sum_{k=0}^{m-1} \mathbf{B}_{\mathbf{m}-\mathbf{k}} \begin{pmatrix} \boldsymbol{\phi}_\mathbf{k} \\ \overline{\boldsymbol{\psi}}_\mathbf{k} \end{pmatrix} \tag{4.18}$$

and

$$\mathbf{B_m} = \mathbf{B}\left(\frac{\delta(\zeta_m)}{\Delta t}\right).$$

In addition, $\delta(\zeta_m) = (1-\zeta_m) + \frac{1}{2}(1-\zeta_m)^2$ is the generating function of the second-order backward differentiation formula (BDF2). We adopt the choice of ζ_m from Kielhorn and Schanz[14] given by $\zeta_m = R\exp\left(\frac{2\pi i m}{n_{\max}}\right)$ with $R = 10^{-\frac{5}{2n_{\max}}}$ and $n_{\max}$ the maximal number of time steps.

Here, the second term of (4.18) contains all the information of the boundary densities up to the previous time step $m-1$ and the first term represents the prescribed boundary densities, if they exist (for more information, see Kielhorn[13]). Since $\overline{\boldsymbol{\psi}}^{n+\frac{1}{2}} = \frac{1}{2}(\boldsymbol{\psi}^{n+1} + \boldsymbol{\psi}^n)$ and $\boldsymbol{\phi}^{n+\frac{1}{2}} = \frac{1}{2}(\boldsymbol{\phi}^{n+1} + \boldsymbol{\phi}^n)$, we find

$$\mathbf{B_0}\begin{pmatrix}\boldsymbol{\phi}^{n+\frac{1}{2}}\\ \overline{\boldsymbol{\psi}}^{n+\frac{1}{2}}\end{pmatrix} = \frac{1}{2}\left(\begin{pmatrix}\mathbf{b}^{\phi}_{\mathbf{n+1}}\\ \mathbf{b}^{\psi}_{\mathbf{n+1}}\end{pmatrix} + \begin{pmatrix}\mathbf{b}^{\phi}_{\mathbf{n}}\\ \mathbf{b}^{\psi}_{\mathbf{n}}\end{pmatrix}\right) =: \begin{pmatrix}\mathbf{b}^{\phi}_{\mathbf{n+\frac{1}{2}}}\\ \mathbf{b}^{\psi}_{\mathbf{n+\frac{1}{2}}}\end{pmatrix}.$$

All in all, we have to solve the system

$$(\mathbf{B_0} + \triangle t\mathbf{G})\begin{pmatrix}\boldsymbol{\phi}^{n+\frac{1}{2}}\\ \overline{\boldsymbol{\psi}}^{n+\frac{1}{2}}\end{pmatrix} = \boldsymbol{\chi}^n$$

with

$$\mathbf{G} = \begin{pmatrix}\frac{1}{2}\frac{1}{\rho}\mathbf{C_0^T}\mathbf{M_0^{-1}}\mathbf{C_0} & 0\\ 0 & 2\mu\alpha\mathbf{C_1^T}\mathbf{M_1^{-1}}\mathbf{C_1} + 2\lambda\alpha\overline{\mathbf{C}}_\mathbf{1}^\mathbf{T}\mathbf{M_2^{-1}}\overline{\mathbf{C}}_\mathbf{1}\end{pmatrix}$$

and

$$\boldsymbol{\chi}^n = \begin{pmatrix}\mathbf{b}^{\Phi}_{\mathbf{n+\frac{1}{2}}}\\ \mathbf{b}^{\Psi}_{\mathbf{n+\frac{1}{2}}}\end{pmatrix} + \begin{pmatrix}\mathbf{C_0^T}\overline{\mathbf{u}}^{n+\frac{1}{2}}\\ \mu\mathbf{C_1^T}\left(\mathbf{V}^{n+\frac{1}{2}} - \alpha\triangle t^2\mathbf{M_1^{-1}}\mathbf{C_1}\dot{\boldsymbol{\psi}}^{n+\frac{1}{2}}\right) + \lambda\overline{\mathbf{C}}_\mathbf{1}^\mathbf{T}\left(\boldsymbol{\omega}^{n+\frac{1}{2}} - \alpha\triangle t^2\mathbf{M_2^{-1}}\overline{\mathbf{C}}_\mathbf{1}\dot{\boldsymbol{\psi}}^{n+\frac{1}{2}}\right)\end{pmatrix}$$

in order to calculate $\boldsymbol{\phi}^{n+\frac{1}{2}}$ and $\overline{\boldsymbol{\psi}}^{n+\frac{1}{2}}$.

At last the convolution quadrature allows us to calculate a feasible initial solution $\ddot{\mathbf{u}}^0$, $\dot{\boldsymbol{\phi}}^0$, $\dot{\boldsymbol{\psi}}^0$ for the initial values $\mathbf{u}^0$, $\dot{\mathbf{u}}^0$, $\dot{\mathbf{f}}$ and, in extension, the initial values $\boldsymbol{\phi}$ and $\boldsymbol{\psi}$ due to their definition. Hence, we take a look at the second order formulation

$$\rho\mathbf{M_0}\ddot{\mathbf{u}} = -\mu\mathbf{D^T}\mathbf{M_1^{-1}}(\mathbf{Du} - \mathbf{C_1}\boldsymbol{\psi}) - \lambda\overline{\mathbf{D}}\mathbf{M_2^{-1}}(\overline{\mathbf{D}}^\mathbf{T}\mathbf{u} + \overline{\mathbf{C}}_\mathbf{1}\boldsymbol{\psi}) - \mathbf{C_0}\dot{\boldsymbol{\phi}} + \rho\mathbf{M_0}\dot{\mathbf{f}}, \tag{4.19}$$

$$\mathbf{B}(\partial_t)\begin{pmatrix}\dot{\boldsymbol{\phi}}\\ \dot{\boldsymbol{\psi}}\end{pmatrix} = \begin{pmatrix}\mathbf{C_0^T}\dot{\mathbf{u}}\\ \mu\mathbf{C_1^T}\mathbf{M_1^{-1}}(\mathbf{Du} - \mathbf{C_1}\boldsymbol{\psi}) - \lambda\overline{\mathbf{C}}_\mathbf{1}^\mathbf{T}\mathbf{M_2^{-1}}(\overline{\mathbf{D}}^\mathbf{T}\mathbf{u} + \overline{\mathbf{C}}_\mathbf{1}\boldsymbol{\psi})\end{pmatrix} \tag{4.20}$$

obtained by inserting $\dot{\mathbf{V}}$ and $\dot{\boldsymbol{\omega}}$ in (3.2)-(3.5). This leads to the linear system of equations

$$\begin{pmatrix}-\rho\mathbf{M_0} & -\mathbf{C_0} & \mathbf{0}\\ \mathbf{0} & \frac{\delta(\zeta_0)}{\triangle t}\mathbf{J}\left(\frac{\delta(\zeta_0)}{\triangle t}\right) & \mathbf{K^T}\left(\frac{\delta(\zeta_0)}{\triangle t}\right)\\ \mathbf{0} & -\mathbf{K}\left(\frac{\delta(\zeta_0)}{\triangle t}\right) & \frac{\triangle t}{\delta(\zeta_0)}\mathbf{W}\left(\frac{\delta(\zeta_0)}{\triangle t}\right)\end{pmatrix}\begin{pmatrix}\ddot{\mathbf{u}}\\ \dot{\boldsymbol{\phi}}\\ \dot{\boldsymbol{\psi}}\end{pmatrix} \tag{4.21}$$

$$= \begin{pmatrix}-\rho\mathbf{M_0}\dot{\mathbf{f}} + \mu\mathbf{D^T}\mathbf{M_1^{-1}}(\mathbf{Du} - \mathbf{C_1}\boldsymbol{\psi}) + \lambda\overline{\mathbf{D}}\mathbf{M_2^{-1}}(\overline{\mathbf{D}}^\mathbf{T}\mathbf{u} + \overline{\mathbf{C}}_\mathbf{1}\boldsymbol{\psi})\\ \mathbf{C_0^T}\dot{\mathbf{u}}\\ \mu\mathbf{C_1^T}\mathbf{M_1^{-1}}(\mathbf{Du} - \mathbf{C_1}\boldsymbol{\psi}) - \lambda\overline{\mathbf{C}}_\mathbf{1}^\mathbf{T}\mathbf{M_2^{-1}}(\overline{\mathbf{D}}^\mathbf{T}\mathbf{u} + \overline{\mathbf{C}}_\mathbf{1}\boldsymbol{\psi})\end{pmatrix}.$$

FIGURE 1 L-shaped domain for the numerical experiments

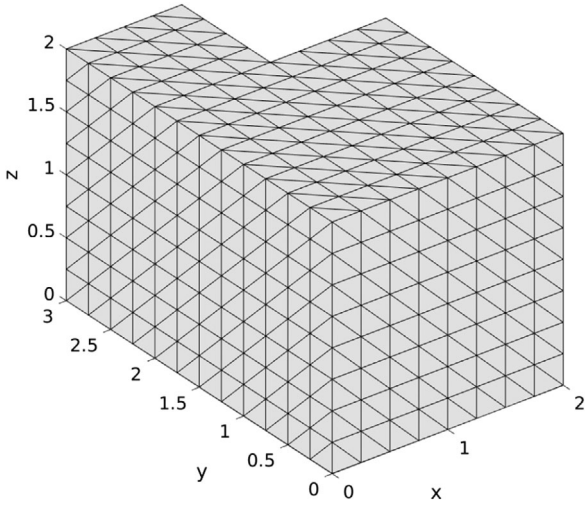

In order to calculate the entries of this matrix, the generating matrices $\mathbf{M_0}$, $\mathbf{M_1}$, $\mathbf{M_2}$, $\mathbf{D}$, $\overline{\mathbf{D}}$ as well as $\mathbf{C_0}$, $\mathbf{C_1}$, $\overline{\mathbf{C}}_\mathbf{1}$ and $\mathbf{J}$, $\mathbf{K}$, $\mathbf{W}$ as introduced in the previous part are required. Given the initial values $\mathbf{u}$, $\dot{\mathbf{u}}$, $\dot{\mathbf{f}}$, we are able to determine the initial values $\ddot{\mathbf{u}}$, $\dot{\boldsymbol{\phi}}$, $\dot{\boldsymbol{\psi}}$ by the inversion of (4.21).

Remark 3. Summarizing the steps of the implementation, we end up with the following algorithm

1. Initialize the input data.
2. Generate the meshes for the triangles and tetrahedra.
3. Calculate the entries of the generating matrix (4.21).
4. Solve the system for the initial solution.
5. Perform the convolution quadrature to get $\boldsymbol{\phi}^{n+\frac{1}{2}}$, $\overline{\boldsymbol{\psi}}^{n+\frac{1}{2}}$.
6. Use the results for the leapfrog scheme.
7. Return to 5. until a predefined time step is reached.

5 | NUMERICAL EXAMPLE

As stated in the introduction, our numerical method can be applied for non-convex domains. Thus, we consider a simple example to get a better insight and choose an L-shaped domain. For the corresponding numerical experiments, we use a medium with the parameters $\lambda = 5.7692 \cdot 10^4$ Pa, $\mu = 3.8462 \cdot 10^4$ Pa, $\rho = 7860\ \frac{\text{kg}}{\text{m}^3}$, $\alpha = 1$.

First, the grid width of the L-shaped domain Ω is chosen to be $h = 0.25$ m and the time steps are given by $\triangle t = 10^{-1} \cdot 2^{-i}$ s, $i = 0, \dots, 4$. Figure 1 shows the domain under consideration. The inhomogeneity f is chosen as

$$f(x,t) = \begin{cases} \left(0, \left(1 - \frac{|x-c|}{\tau}\right)^2 \cdot \left(\frac{2|x-c|}{\tau} + 1\right), 0\right)^T \cdot \frac{(t_0-t)^5}{t_0^5}, & t \le t_0,\ |x-c| \le \tau \\ (0,0,0)^T, & \text{else} \end{cases} \quad \text{in } \Omega,$$

where $c = (1,1,1)^T$, $\tau = 1$ and $t_0 = 0.5$ s. For the visualization, we take a look at the second component $u_2(x,t)$ of the solution vector $u(x,t)$ in $t \in [0,T]$ at the fixed points

- (1,1,1), i.e., an interior point,
- (0,1,1), i.e., a point at the boundary,
- (1,2,1), i.e., a point on an edge.

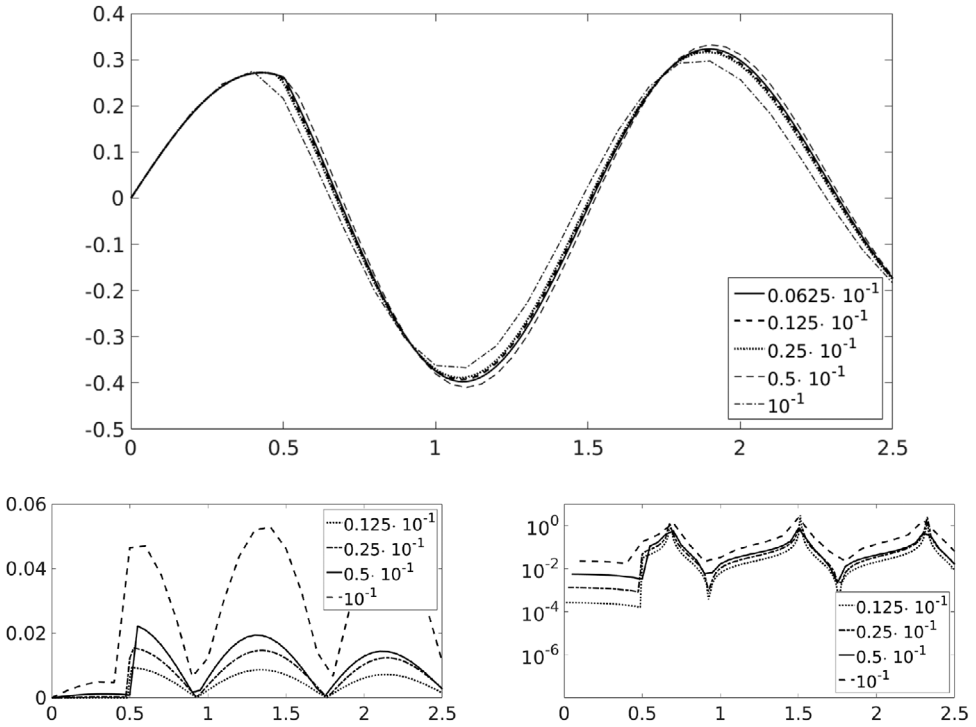

FIGURE 2 Solution $u_2((1,1,1)^T,t)$ (top) and the errors (bottom) for different Δt in seconds (left hand side the absolute error and right hand side the relative error)

In addition, we compare the solutions $u_2^{\Delta t}(x,t)$ for $\Delta t = 10^{-1}$ s, $\Delta t = 0.5 \cdot 10^{-1}$ s, $\Delta t = 0.25 \cdot 10^{-1}$ s and $\Delta t = 0.125 \cdot 10^{-1}$ s with the solution $\tilde{u}_2(x,t)$ for $\Delta t = 0.0625 \cdot 10^{-1}$ s. In absence of an analytical solution, we examine the different realizations by presenting the relative error

$$\mathcal{E}_{rel}(x,t) = \frac{|\tilde{u}(x,t) - u^{\Delta t}(x,t)|}{|\tilde{u}(x,t)|}$$

and the absolute error

$$\mathcal{E}_{abs}(x,t) = |\tilde{u}(x,t) - u^{\Delta t}(x,t)|.$$

Figures 2–4 show the solution and the corresponding absolute and relative error plots for different time step sizes ($\Delta t = 10^{-1}$ s, $\Delta t = 0.5 \cdot 10^{-1}$ s, $\Delta t = 0.25 \cdot 10^{-1}$ s, $\Delta t = 0.125 \cdot 10^{-1}$ s and $\Delta t = 0.0625 \cdot 10^{-1}$ s) and a fixed grid width $h = 0.25$ m.

The figures are organized as follows: on the top, the solution at a fixed point for different Δt is shown, while the point of consideration is stated in the caption. At the bottom, the absolute error (left hand side) and relative error (right hand side) are given.

We chose $h = 0.25$ m, since the experiments with different h as depicted in Figures 5–7 show that for this choice, we obtain a solution close enough to $\tilde{u}(x,t)$ for a reasonable numerical effort. We set f in such a way that it decreases until $t_0 = 0.5$ to zero. In more detail, we conclude that the time discretization methods (leapfrog in the interior and convolution quadrature with BDF2 on the boundary) is stable for sufficiently small time steps. We observe for the solution in the interior (Figure 2) as well as for the solution on the boundary (Figures 3 and 4), that both absolute and relative error decreases with a smaller time step size. We want to remark, that the large relative errors occur only for small amplitudes, where the values are close to zero. Conversely, the absolute error is small. All in all, this illustrates the convergence of the approximated solution, since the error decreases with lower step sizes.

After examinating the solution for different time step sizes, we go over to the examination of different grid sizes $h = \frac{1}{n}$ m and a fixed $\Delta t = 0.25 \cdot 10^{-1}$ s, since this choice provides a sufficiently good approximation of the solution for a reasonable numerical effort. For the analysis of the behavior for different h, we take a look at $n = 2$, $n = 4$, $n = 6$ and $n = 8$ by showing that both absolute and relative error decrease while choosing a larger n. For $n = 2$ the errors are relative large and thus only presents an

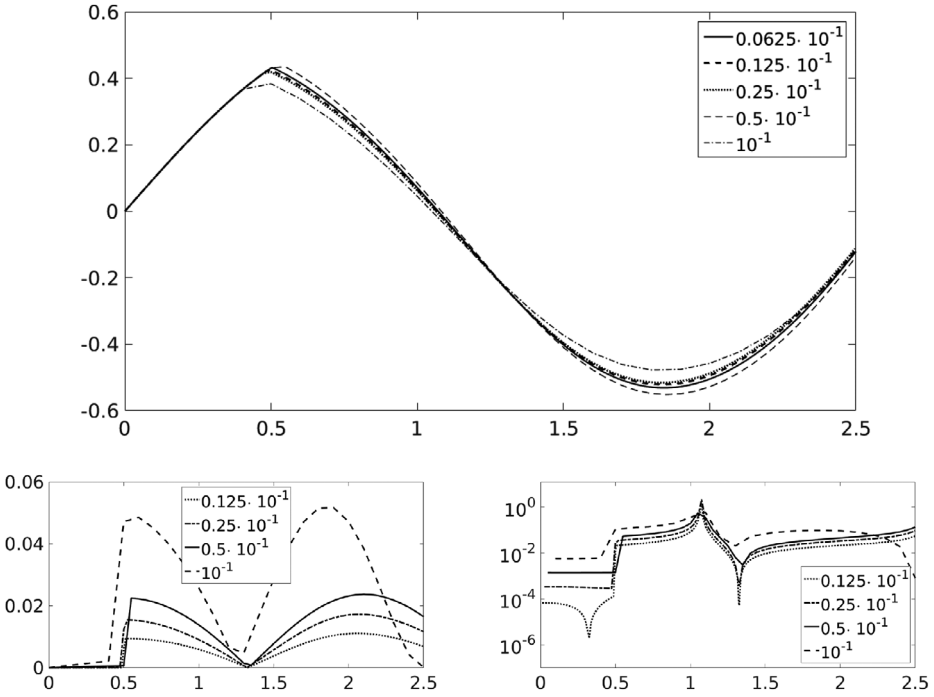

FIGURE 3 Solution $u_2((0,1,1)^T,t)$ (top) and the errors (bottom) for different $\triangle t$ in seconds (left hand side the absolute error and right hand side the relative error)

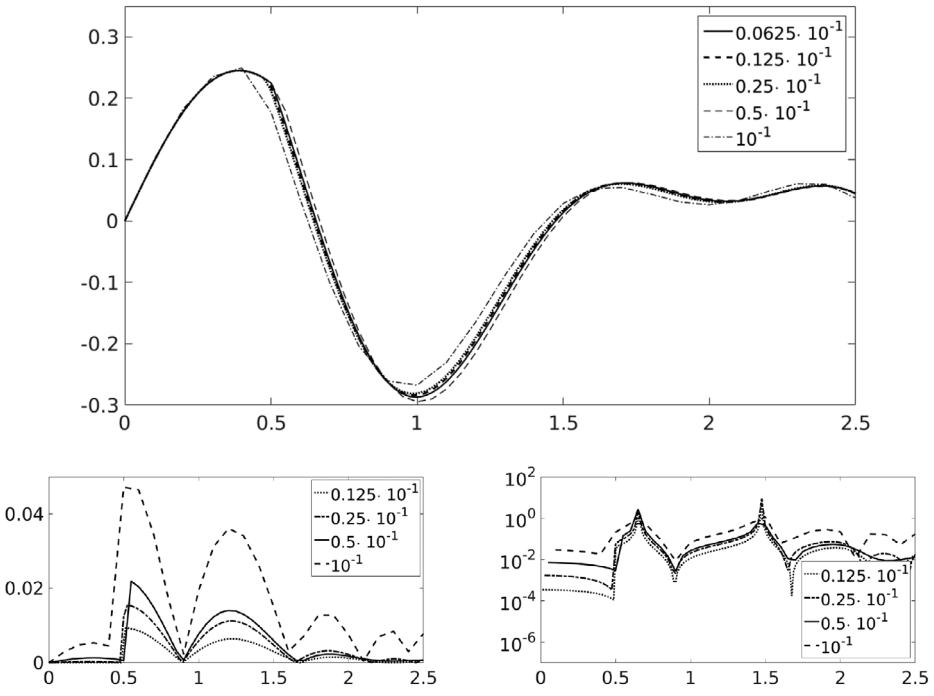

FIGURE 4 Solution $u_2((1,2,1)^T,t)$ (top) and the errors (bottom) for different $\triangle t$ in seconds (left hand side the absolute error and right hand side the relative error)

upper bound on h. Similar as in Figure 2–Figure 4 we observe that for a finer triangulation, the solutions are close to each other. The error plots reflect this behavior.

Again, the figures are organized as follows: on the top the solution for a fixed $\triangle t = 0.25 \cdot 10^{-1}$ s and different n is presented. At the bottom, the absolute error (left hand side) and relative error (right hand side) are given with a semi logarithmic scale. In addition the different parameters n are included in the plots themselves.

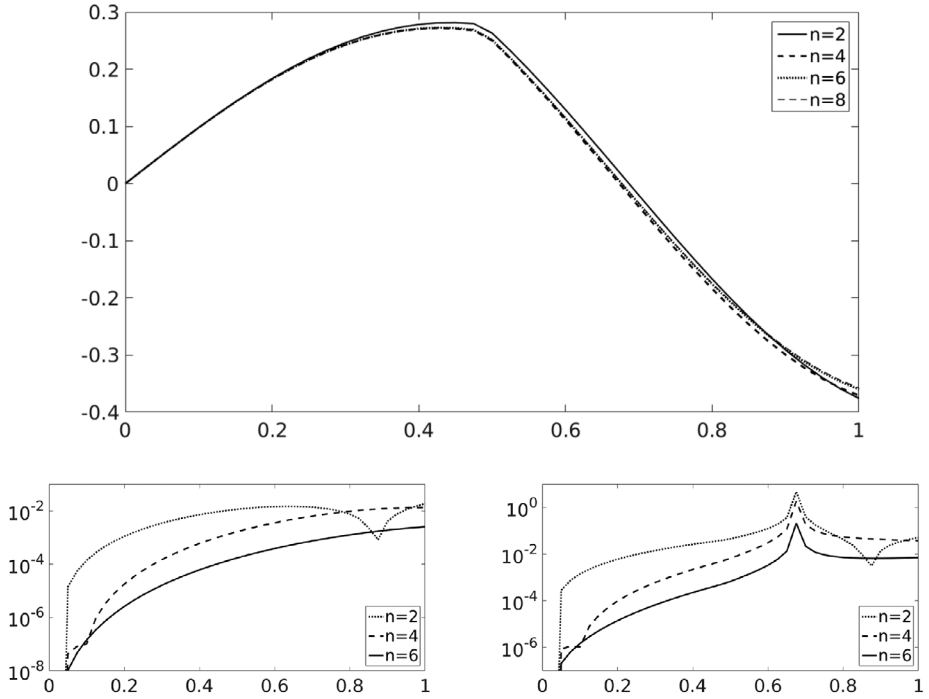

FIGURE 5 Solution $u_2((1,1,1)^T,t)$ (top) and the errors (bottom) for different $h = \frac{1}{n}$ m (left hand side the absolute error and right hand side the relative error)

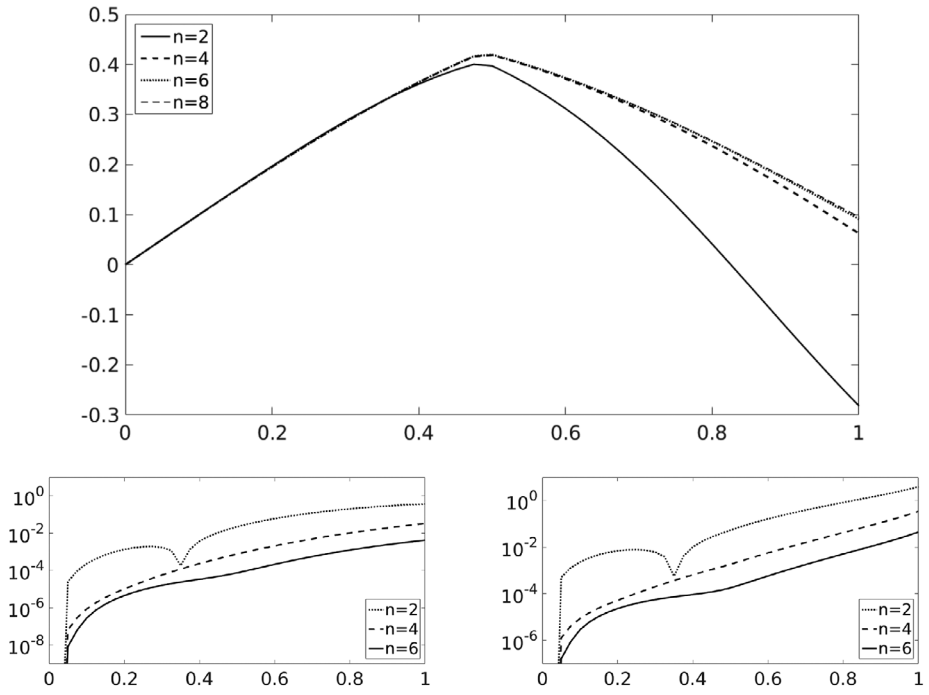

FIGURE 6 Solution $u_2((0,1,1)^T,t)$ (top) and the errors (bottom) for different $h = \frac{1}{n}$ m (left hand side the absolute error and right hand side the relative error)

Finally, we combine the discretization refinement in space and time. In the following numerical experiment, the reference solution is calculated for $h = \frac{1}{8}$ m and $\Delta t = \frac{1}{8} \cdot 10^{-1}$ s. The results for different grid widths $h = \frac{1}{n}$ m and the corresponding time steps $\Delta t = \frac{1}{n} \cdot 10^{-1}$ s are shown in Figure 8 (top). In addition, we plot the absolute and relative error w.r.t. the reference solution at the bottom of Figure 8.

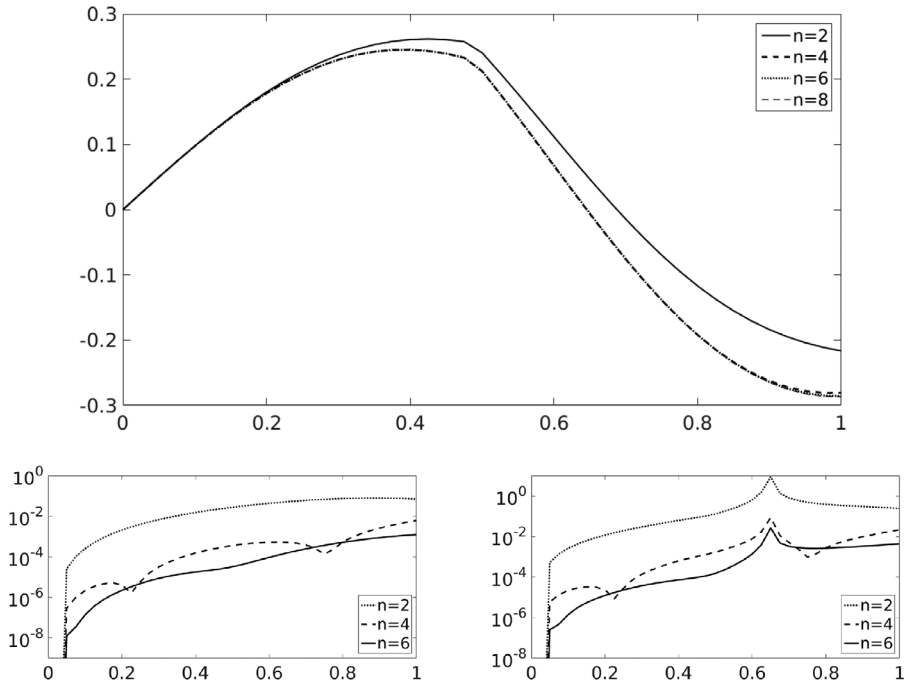

FIGURE 7 Solution $u_2((1,2,1)^T,t)$ (top) and the errors (bottom) for different $h = \frac{1}{n}$ m (left hand side the absolute error and right hand side the relative error)

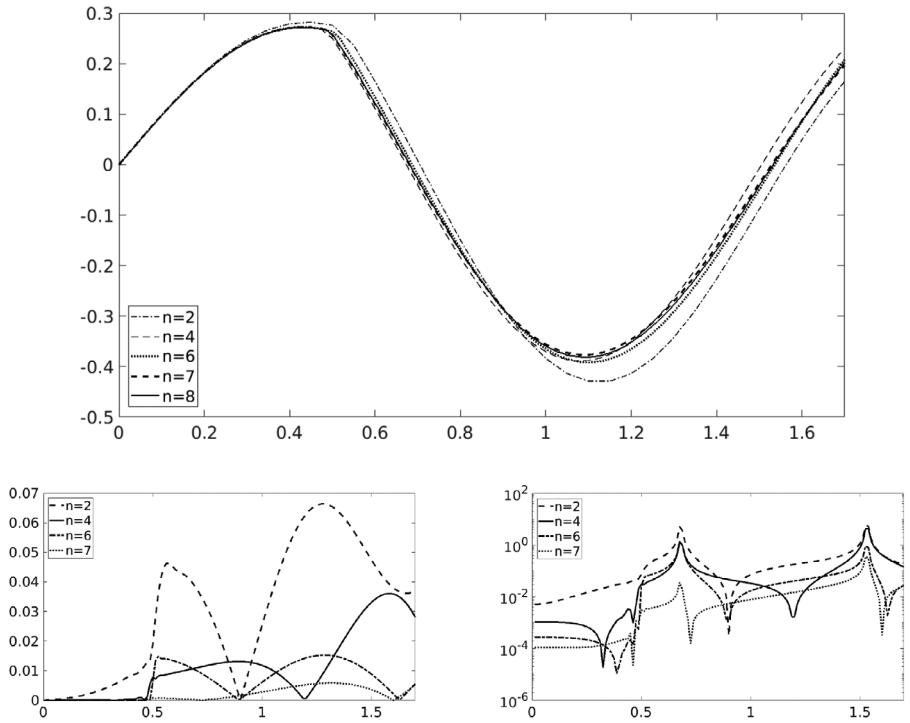

FIGURE 8 Solution $u_2((1,1,1)^T,t)$ (top) and the errors (bottom) for different $h = \frac{1}{n}$ m and $\Delta t = \frac{1}{n} \cdot 10^{-1}$ s (left hand side the absolute error and right hand side the relative error)

Summarizing the results of our numerical experiments, Figure 8 illustrates the numerical convergence of our FEM-BEM-coupling and the corresponding time-discretization with leapfrog and convolution quadrature.

In fact, Figure 9 shows that the convergence rate $\mathcal{O}(\Delta t^2 + h)$ is obtained. In more detail, we take a look at a loglog representation of the maximal absolute errors for the simultaneous refinement in space and time and compare this with the reference line

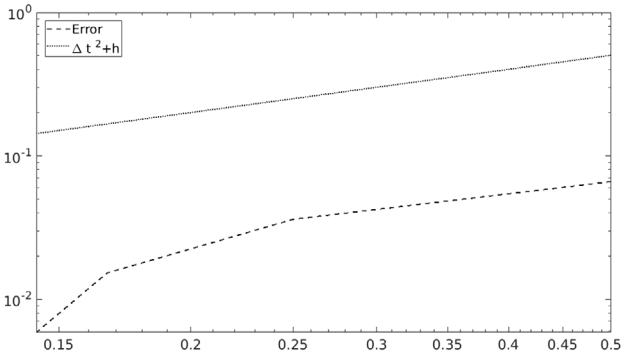

FIGURE 9 Convergence rate for the solution $u_2((1,1,1)^T,t)$

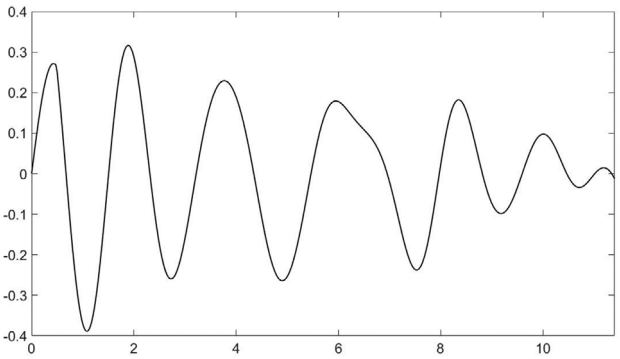

FIGURE 10 Solution $u_2((1,1,1)^T,t)$ for $\triangle t = 0.25 \cdot 10^{-1}$ s and $h = 0.25$ m

for $\Delta t^2 + h$. We observe that indeed the error plot is approximately parallel to the reference line, which shows the numerical convergence of our method as presented in the theoretical result (Theorem 4).

At last, in order to show the longtime behavior of the solution, we exemplary take a look at the solution for $\triangle\, t = 0.25 \cdot 10^{-1}$ s and $h = 0.25$ m in the time intervall $[0, 12]$ s (cf. Figure 10). As expected, we observe the decay of the solution to zero.

6 | CONCLUSION AND OUTLOOK

We started with a summary of the theoretical background of the interior-exterior coupling for the elastodynamic wave equation in 3D and introduced the numerical methods. We used boundary elements and convolution quadrature on the boundary and finite elements and leapfrog in the interior. In addition, we took a look at the convergence of these methods. Based on this, we stated the details of the implementation, where we focused on the construction of the corresponding matrices and the performance of the time discretization. In the last section, we presented the numerical examples for an L-shaped domain. We divided our considerations into the examination of different time step sizes with a fixed grid width and the examination of different grid widths for a fixed time step size. All in all, the figures and corresponding plots showed us the numerical convergence of the methods.

ACKNOWLEDGEMENTS

The author would like to thank the anonymous reviewers for the helpful remarks and suggestions for the improvement of the paper.

REFERENCES

[1] J. Alberty, C. Carstensen, S. A. Funken, R. Klose, Matlab implementation of the finite element method in elasticity, *Computing, Springer* **2002**, *69*, 239.

[2] M. S. Alnaes, J. Blechta, J. Hake, A. Johansson, B. Kehlet, A. Logg, C. Richardson, J. Ring, M. E. Rognes, G. N. Wells, The fenics project version 1.5, *Archive of Numerical Software* **2015**, *3*.

[3] B. Aour, O. Rahmani, M. Nait-Abdelaziz, A coupled FEM/BEM approach and its accuracy for solving crack problems in fracture mechanics, *Int. J. Solids Struct.* **2007**, *44*, 2523.

[4] L. Banjai, Ch. Lubich, F.-J. Sayas, Stable numerical coupling of exterior and interior problems for the wave equation, *Numer. Math.* **2015**, *129*, 611.
[5] C. Carstensen, S. Funken, E. Stephan, On the adaptive coupling of FEM and BEM in 2-d-elasticity, *Numer. Math.* **1997**, *77*, 187.
[6] D. Clouteau, M. L. Elhabre, D. Aubry, Periodic BEM and FEM-BEM coupling - Application to seismic behaviour of very long structures, *Comput. Mech.* **2000**, *25*, 567.
[7] V. Domínguez, T. Sánchez-Vizuet, F.-J. Sayas, A fully discrete Calderón calculus for the two-dimensional elastic wave equation, *Computers and Mathematics with Applications* **2015**, *69*, 620.
[8] S. Eberle, The elastic wave equation and the stable numerical coupling of its interior and exterior problems, *ZAMM* **2018**, *98*, 1261.
[9] O. V. Estorff, H. Antes, On FEM-BEM coupling for fluid structure interaction analysis in the time domain, *Int. J. Numer. Methods Engrg.* **1991**, *31*, 1151.
[10] C. Felippa, *The linear tetrahedron*. In *Advanced Finite Element Methods (Lecturenotes)*. Department of Aerospace Engineering Sciences, University of Colorado at Boulder **2017**.
[11] P. Jean, A 3D FEM/BEM code for ground-structure interaction: Implementation strategy including the multi-traction problem, *Eng. Anal. Bound. Elem.* **2015**, *69*, 52.
[12] M. Kerdjouj, F. M. L. Amirouche, Implementation of the boundary element method in the dynamics of flexible bodies, *Int. J. Numer. Methods Engrg.* **1996**, *39*, 321.
[13] L. Kielhorn, *A Time-Domain Symmetric Galerkin BEM for Viscoelastodynamics*. Monographic Series TU Graz, Computation in Engineering and Science, Vol. 5, **2009**.
[14] L. Kielhorn, M. Schanz, Convolution quadrature method-based on symmetric Galerkin boundary element method for 3-d elastodynamics, *Int. J. Numer. Engng.* **2008**.
[15] H.-B. Li, G.-M. Han, H. Mang, Y. P. Torzchy, A new method for the coupling of finite element and boundary element discretized subdomains of elastic bodies, *Comput. Methods Appl. Mech.* **1986**, *54*, 161.
[16] F. Rammerstorfer, M. Schanz., FEM-BEM coupling with non-conforming interfaces, *PAMM* **2011**, *11*, 487.
[17] T. Rüberg, M. Schanz, Coupling finite and boundary element methods for static and dynamic elastic problems with non-conforming interfaces, *Comput. Methods Appl. Mech. Engrg.* **2008**, *198*, 449.
[18] F.-J. Sayas, *Retarded Potentials and Time Domain Boundary Integral Equations. A Road Map*. Springer Series in Computational Mathematics 50. Springer, **2016**.
[19] H. Ziegelwanger, P. Reiter, M. Conter, The three-dimensional quasi-periodic boundary element method: implementation, evaluation, and use cases, *Int. J. Comp. Meth. and Exp. Meas* **2017**, *5*, 404.
[20] O. C. Zienkiewicz, D. W. Kelly, P. Bettess, The coupling of the finite element method and boundary solution procedures, *Int. J. Numer. Methods Engrg.* **1977**, *11*, 355.

How to cite this article: S. Eberle. An implementation and numerical experiments of the FEM-BEM coupling for the elastodynamic wave equation in 3D. *Z Angew Math Mech*. 2019;99:e201900050. https://doi.org/10.1002/zamm.201900050